Optical properties of Titan and early Earth haze laboratory analogs in the mid-visible

Christa A. Hasenkopf [a,b,*], Melinda R. Beaver [b,c], Melissa G. Trainer [d], H. Langley Dewitt [b,c], Miriam A. Freedman [b], Owen B. Toon [a,e], Christopher P. McKay [f], Margaret A. Tolbert [b,c]

[a] Department of Atmospheric and Oceanic Sciences, University of Colorado, Boulder, CO 80309, United States
[b] Cooperative Institute for Research in the Environmental Sciences, University of Colorado, Boulder, CO 80309, United States
[c] Department of Chemistry, University of Colorado, Boulder, CO 80309, United States
[d] NASA Goddard Space Flight Center, Greenbelt, MD 20771, United States
[e] Laboratory for Atmospheric and Space Physics, University of Colorado, Boulder, CO 80309, United States
[f] Space Science Division, NASA Ames Research Center, Moffett Field, CA 94503, United States

ARTICLE INFO

ABSTRACT

Scattering and absorption of sunlight by aerosols are integral to understanding the radiative balance of any planetary atmosphere covered in a haze, such as Titan and possibly the early Earth. One key optical parameter of an aerosol is its refractive index. We have simulated both Titan and early Earth organic haze aerosols in the laboratory and measured the real and imaginary portion of their refractive index at $\lambda = 532$ nm using cavity ringdown aerosol extinction spectroscopy. This novel technique allows analysis on freely-floating particles minutes after formation. For our Titan analog particles, we find a real refractive index of $n = 1.35 \pm 0.01$ and an imaginary refractive index $k = 0.023 \pm 0.007$, and for the early Earth analog particles we find $n = 1.81 \pm 0.02$ and $k = 0.055 \pm 0.020$. The Titan analog refractive index has a smaller real and similar imaginary refractive index compared to most previous laboratory measurements of Titan analog films, including values from Khare et al. (Khare, B.N., Sagan, C., Arakawa, E.T., Suits, F., Callcott, T.A., Williams, M.W. [1984]. Icarus 60, 127–137). These newly measured Titan analog values have implications for spacecraft retrievals of aerosol properties on Titan. The early Earth analog has a significantly higher real and imaginary refractive index than Titan analogs reported in the literature. These differences suggest that, for a given amount of aerosol, the early Earth analog would act as a stronger anti-greenhouse agent than the Titan analog.

1. Introduction

Organic hazes are prevalent throughout the Solar System. They have been identified in the atmospheres of Jupiter (Hord et al., 1979; Kim et al., 1985), Saturn (Gillett and Forrest, 1974), Uranus (Burgdorf et al., 2006), Neptune (Moses et al., 1995), and, perhaps most famously, Saturn's moon Titan (Smith et al., 1981; Tomasko et al., 2005). On Titan, a globally-ubiquitous hydrocarbon haze is generated from ultraviolet (UV) photolysis and electron initiated dissociation of methane (CH_4), nitrogen (N_2), and other trace species (Cabane and Chassefiere, 1995). The organic particles formed from these processes have a profound effect on the radiative balance of the titanian atmosphere and surface temperature. Because the haze efficiently absorbs solar radiation, it produces an inversion in the atmospheric temperature profile of Titan. The haze acts as an anti-greenhouse agent, keeping the surface roughly 10% cooler than it would be without its presence (McKay et al., 1991). The opacity or transparency of any haze to a given wavelength of light is dictated by the aerosol size distribution, particle shape, and chemical composition. Chemical composition of the haze controls the optical properties of the aerosol – namely, the real and imaginary portions of its refractive index. The refractive index of Titan haze aerosol is needed to interpret spacecraft retrievals that determine several properties of Titan aerosol, including particle size and single-scattering albedo as a function of altitude (Tomasko et al., 2005).

Several laboratory studies on optical constants of Titan haze exist (Khare et al., 1984; Ramirez et al., 2002; Tran et al., 2003; Vuitton et al., 2009). These works have generated Titan aerosol analogs by exposing various Titan-relevant gas mixtures to either ion discharge sources or a UV emission line lamp. All of the previous studies collected the haze analog over long periods of time, on the order of hours to days, as thin films for analysis. These studies have resulted in the retrieval of imaginary refractive indices in the mid-visible that vary by over an order of magnitude.

Several workers have suggested the existence of a Titan-like haze on the early Earth (Kasting et al., 1983; Sagan and Chyba,

* Corresponding author. Address: Cooperative Institute for Research in the Environmental Sciences, University of Colorado, Boulder, CO 80309, United States. Fax: +1 303 492 1149.
E-mail address: Christa.Hasenkopf@colorado.edu (C.A. Hasenkopf).

1997; Zahnle, 1986). Such a haze might form if the early Earth atmosphere had higher than present day levels of CH_4 and carbon dioxide (CO_2). While such greenhouse gases could offer a solution to the Faint Young Sun Paradox (Kasting et al., 1983; Sagan and Chyba, 1997), they could also form a Titan-like haze with a possible anti-greenhouse effect (Haqq-Misra et al., 2008; McKay et al., 1991; Pavlov et al., 2001a). CO_2 has a comparable absorption cross-section to that of CH_4 in the UV range, suggesting it could alter the rate of haze production and haze chemical composition from that observed on Titan. A recent model of the early Earth atmosphere predicts an organic haze with a significant optical depth will form in atmospheres with CH_4/CO_2 as low as 0.1 (Domagal-Goldman et al., 2008). Laboratory work corroborates these results. For example, Dewitt et al. (2009) report measurable aerosol generation from atmospheres with $CH_4/CO_2 \geqslant 0.1$.

Mass spectra of the aerosols produced from UV-irradiated Titan and early Earth atmosphere analogs show that the two aerosols are chemically different. Fig. 1a illustrates this by comparing mass spectra of typical Titan and early Earth aerosol analogs from Trainer et al. (2006). The Titan analog was made from a UV-irradiated 0.1% CH_4 in N_2 gas mixture, while the early Earth analog was produced by photolysis of a mixture of 0.1% CH_4 and 0.1% CO_2 in N_2. The spectra have been normalized to the total mass signal produced by each analog between $m/z = 20$ amu and 120 amu. The "picket fence" structure in both analog aerosol mass spectra is indicative of particles composed of aliphatic hydrocarbons. Markers of the presence of aliphatic hydrocarbons are seen at $m/z = 41$ amu and at 14 amu ($-CH_2-$) unit intervals ($m/z = 55$ amu, 69 amu, 83 amu, etc.). Also, there is evidence of inclusion of small amounts of aromatics such as benzene ($m/z = 77$ amu) and toluene ($m/z = 91$ amu) fragments in both spectra. The presence of these aromatics is larger relative to the total mass in the Titan aerosol

analog spectrum than the early Earth analog aerosol spectrum. There is a factor of two to three larger mass signal at m/z's 28 amu (CO^+), 30 amu (CH_2O^+), 44 amu (COO^+), and 58 amu ($C_3H_6O^+$) in the early Earth analog aerosol spectrum compared to the Titan analog aerosol mass spectrum. All four of these peaks are markers for oxygen incorporation into the particles and may represent carboxylic acid, ester, or ether groups (Trainer et al., 2006). These differences between the two spectra are highlighted in Fig. 1b, which shows the early Earth mass spectrum subtracted from the normalized Titan mass spectrum. Chemical differences imply that the two aerosols have different optical properties. The optical properties of early Earth haze aerosol analogs have not been previously reported in the literature, requiring models of the early Earth atmosphere to assume that the haze aerosol have the same optical properties as Titan analog aerosol (Domagal-Goldman et al., 2008; Pavlov et al., 2001a).

In the present study, we have generated Titan and early Earth analog aerosols by exposing atmospheric analogs to a continuum UV source. We then used cavity ringdown aerosol extinction spectroscopy (CRD-AES) to measure the extinction of these particles at $\lambda = 532$ nm. We report the first measurements of Titan haze analog optical properties in the mid-visible that have been performed *in situ* on freely-floating particles as well as the first optical properties of an early Earth analog aerosol of any kind.

2. Experimental method

2.1. Aerosol generation and size selection

Our Titan atmosphere analog consisted of 0.1% ultra-high purity grade CH_4 in a background of pre-purified N_2. This gas composition, when photolyzed with UV light, produces particles that are chemically and physically similar to analog aerosols generated from a gas mixture with a more Titan-like CH_4 concentration of 2% in N_2. The 0.1% CH_4 mixture provides higher mass signal for our main analysis instrument than other CH_4–N_2 mixtures irradiated by UV light (Trainer et al., 2006). The early Earth analog atmosphere consists of 0.1% CH_4 and 0.1% CO_2 in N_2. This mixture has a C/O ratio of 1 and is considered to be a plausible early Earth analog atmosphere, in terms of both the absolute concentrations of CH_4 and CO_2 and C/O ratio (Haqq-Misra et al., 2008; Pavlov et al., 2000). It lends itself well to comparison with the particles generated from the Titan analog gas mixture since the concentration of CH_4 is the same. Additionally, the highest production rate of both Titan and early Earth analog particles is found with these mixtures, providing our main analysis instrument with enough signal.

Fig. 2 shows a schematic of the experimental setup for the refractive index determination. All experiments were performed at room temperature and a pressure of 630 Torr. The relevant gases that represent the atmospheric analog of interest are introduced into a stainless steel mixing chamber and are allowed to diffusively mix overnight. The analog atmosphere is then flowed at 60 standard cubic centimeters per minute (sccm) into a reaction cell via a Mykrolis FC-2900 Mass Flow Controller. As the analog atmosphere flows through the reaction chamber, it is exposed to radiation from a water-cooled deuterium continuum UV lamp with MgF_2 windows (Hamamatsu Model L1835). The lamp emits photons from 115 nm to 400 nm, peaking at 160 nm and therefore simulates vacuum ultraviolet solar radiation including the Lyman-α line. The irradiation from the lamp initiates aerosol production.

After exiting the reaction chamber, the aerosol flow rate is increased to a total of 300 sccm by adding a dilution flow of pre-purified N_2. The flow of dry, polydisperse aerosol then enters a Differential Mobility Analyzer (TSI Electrostatic Classifier Model
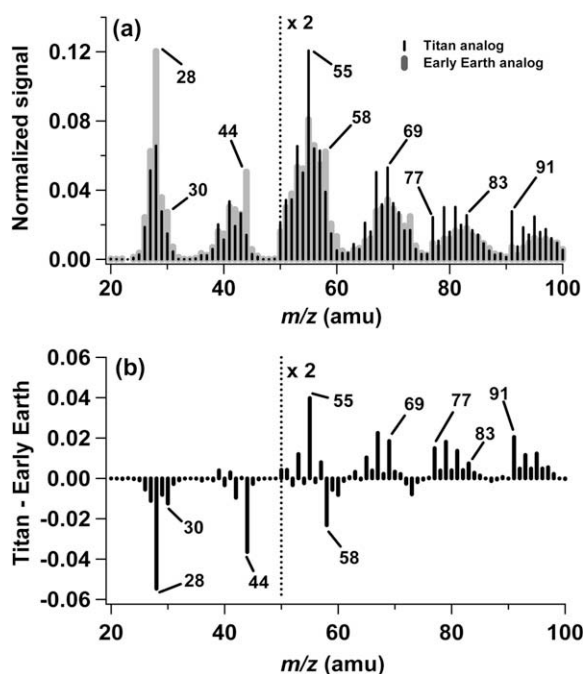

Fig. 1. (a) Averaged aerosol mass spectra for Titan and early Earth analogs. The mass spectra have been normalized to the entire signal between $m/z = 20$ amu and 120 amu. Data to the right of the dashed line at $m/z = 50$ amu are multiplied by 2 for ease of viewing. The black sticks represent mass spectra of Titan aerosol generated from a 0.1% CH_4 in N_2 gas mixture, and the thicker gray sticks represent mass spectra of early Earth aerosol generated from a 0.1% CH_4 and 0.1% CO_2 in N_2 gas mixture. The data are from Trainer et al. (2006). (b) The difference between the Titan and early Earth mass spectra from (a).
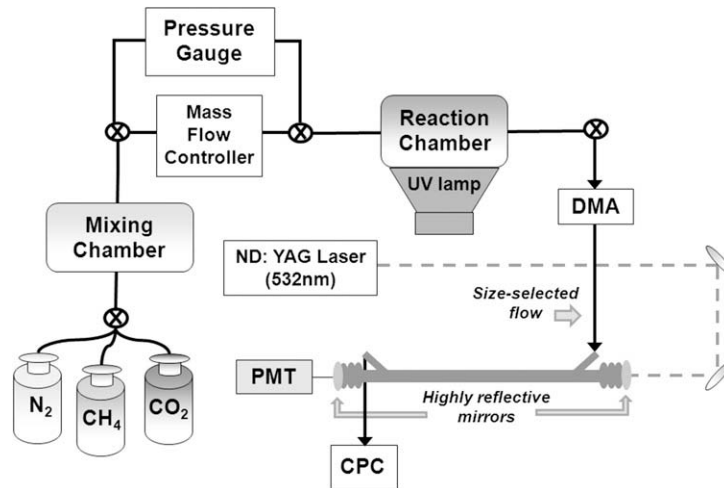
Fig. 2. Schematic of aerosol generation and CRD-AES instrumentation.

3080, DMA), where it is surrounded by a sheath flow of 1500 sccm dry N_2. In the DMA, the flow is exposed to a Kr-85 Bipolar Charger, giving the particles a known bipolar charge distribution. Because the DMA size-selects according to electrical mobility, the exiting flow contains mainly positive singly-charged monodisperse particles. However, the flow also contains a small, but quantifiable population of larger, positive multiply-charged monodisperse particles. The DMA, in conjunction with a Condensation Particle Counter (TSI Model 3022, CPC), was used to measure size distributions of all the aerosols investigated. By selecting particles with sizes larger than the mode diameter of the size distribution, the influence of larger, multiply-charge particles was minimized. We describe our treatment of multiply-charged particles in Section 2.3.

2.2. Cavity ringdown aerosol spectroscopy system

After the size-selected aerosol flow exits the DMA, it enters the CRD-AES. The body of the CRD-AES is a 0.85 m stainless steel tube. Highly reflective ($R > 99.998\%$) mirrors (Advanced Thin Films) are mounted on both ends of the tube. The second harmonic, 532 nm, from a neodymium-doped yttrium aluminum garnet laser (ND:YAG, Big Sky Laser Technologies, Quantel, USA) is pulsed into the cavity and reflects back and forth many times on the mirrors. In a cell with only the background gas (devoid of particles) and over a characteristic timescale τ_o, the intensity of the light falls to $1/e$ of its initial intensity. When measuring τ_o for these experiments, the UV-irradiated gas mixture was flowed through the DMA, which was set to allow no particles through, as confirmed by the CPC. This ensured τ_o included any absorption or Rayleigh scattering from the original gas mixture and from any gases formed from exposure to the UV lamp. However, it should be noted there was no discernible difference between τ_o's observed when the lamp was on or off. A typical τ_o for our cell is 100 μs, which corresponds to an effective pathlength of 30 km. When the cell is filled with aerosol, the ringdown time is decreased to a new ringdown time, τ. The degree to which the ringdown time is decreased is dependent on the concentration and the optical properties of the particles. By comparing the two ringdown times, a measure of the extinction coefficient b_{ext} (cm^{-1}) can be made (Pettersson et al., 2004):

$$b_{ext} = \frac{R_L}{c}\left(\frac{1}{\tau} - \frac{1}{\tau_o}\right) \qquad (1)$$

where R_L is the ratio of the total cavity length (0.85 m) to the cavity length occupied by aerosol sample (0.75 m) and c is the speed of light. After exiting the CRD-AES, the size-selected particles enter a CPC that measures the particle concentration N (number cm^{-3}).

Other optical quantities can be derived from b_{ext} and N, such as the extinction cross-section C_{ext} (cm^2 particle^{-1}) $= b_{ext}/N$. The extinction cross-section C_{ext} represents an effective area over which the particle removes and scatters energy from an incident beam of light. The extinction efficiency Q_{ext} is a measure of how well a beam removes and scatters energy from an incident beam relative to its geometric cross-section, $Q_{ext} = 4C_{ext}/(\pi D^2)$, where D is particle diameter. Analogous optical cross-sections (C) and efficiencies (Q) exist for just the absorption and scattering properties, and are referred later in the text with the subscripts "abs" and "sca," respectively. The single-scattering albedo ($\bar{\omega}$) is the ratio of the extinction due to scattering to the total extinction: $\bar{\omega} = Q_{sca}/Q_{ext}$.

2.3. Refractive index retrieval

It has been verified that both analog aerosols are spherical and chemically homogeneous in Trainer et al. (2006). Therefore, it is appropriate to apply Mie theory to extract the refractive index from our extinction measurements. Mie theory dictates that the extinction of light by a sphere is a function of the incident wavelength of light (λ), the particle diameter, and the refractive index. The refractive index is composed of the real refractive index (n) and the imaginary refractive index (k). We measure or control for all of the parameters mentioned above except for n and k. Therefore, we can compare the measured extinction caused by a concentration of N particles of a particular D with values predicted from Mie theory for a range of n and k. To do this, we used a Mie code written in IDL (Grainger et al., 2004) and that is freely available (http://www.atm.ox.ac.uk/code/mie/index.html) to find the best-fitting refractive indices. Additionally, we take into account the effect of multiply-charged particles.

Multiply-charged particles comprise a small fraction of the size-selected aerosol from the DMA. However, these interfering particles can have a significant influence on the extinction coefficient. By taking extinction measurements starting at sizes much larger than the mode diameter of the aerosol distribution, the influence of triply- and larger-charged particles is insignificant. In the current experiments, doubly-charged particles constitute 1–7% of the size-selected number concentrations. The influence of doubly-charged particles on the extinction is accounted for by calculating their fraction at a given selected size and incorporating that into our model of the extinction,

$$b_{ext} = b_{ext,+1} + b_{ext,+2}$$

$$= (Q_{ext,+1}(n,k,D_{+1},\lambda)D_{+1}^2 f_{+1} + Q_{ext,+2}(n,k,D_{+2},\lambda)D_{+2}^2 f_{+2})\left(\frac{\pi N}{4}\right) \quad (2)$$

where f is the fraction of particles designated as singly- or doubly-charged, and the subscripts +1 and +2 signify singly- or doubly-charged particles. The diameter of the doubly-charged particles, D_{+2}, was measured experimentally by doubling the electrical mobility at the singly-charged diameter and noting what diameter this corresponded to on the DMA. In order to calculate the concentration of doubly-charged particles interfering at a selected singly-charged diameter, the interfering diameter was selected by the DMA and the concentration of particles at this size was measured by the CPC. The concentration measured at this diameter was assumed to be only singly-charged particles, and it was then converted into an interfering doublet concentration at the singly-charged size according to Wiedensohler (1988). The accuracy of these methods to predict the doublet size and interfering concentration was verified experimentally by size-selecting particles through one DMA and sending the size-selected population into a second DMA, which was set to automatically scan all sizes. The particles were then sent to a CPC to count the concentration. The difference between the measured fraction of interference and the values predicted by Wiedensohler (1988) was less than 5%.

To determine which n and k provide the best fit to the observed extinction corrected for doubly-charged particles, we calculate the reduced cumulative fractional difference (CFD$_R$) for a selection of particle sizes. The CFD$_R$ is defined as:

$$CFD_R = \frac{1}{P}\sum_{All\ sizes}\frac{|b_{ext\text{-}measured} - b_{ext\text{-}Mie}|}{b_{ext\text{-}measured}} \quad (3)$$

where P is the number of particle sizes at which the extinction and concentration were measured. The CFD$_R$ measures the absolute value of the average fractional difference in the fit of the extinction for each pair of n and k relative to the measured value. The algorithm tested all n from 1.00 to 2.00 in increments of 0.01, while k was tested from 0.000 to 0.500 in increments of 0.001. A CFD$_R$ value was calculated from extinction coefficient and particle concentration measurements for at least four sizes, termed one "run." The lowest CFD$_R$ value in the entire parameter space determined the best-fitting n and k. By looking at CFD$_R$ contours in n–k space, we verified that the lowest CFD$_R$ values represented unique global minima in the data sets. The reported refractive index values are averages of the best-fitting n and k from at least three runs, and the error reported is the standard deviation of all of the runs of one compound.

3. Results

3.1. Refractive index retrieval for test cases

Two test cases were performed to verify the experimental approach and refractive index retrieval techniques. The first case was for a purely scattering compound, dry ammonium sulfate (Sigma Aldrich). The other case was nigrosin dye (Aldrich, CAS 8005-03-6), which is a scattering and highly absorbing substance. The refractive indices of both materials have been reported previously in the literature.

The test case aerosols were generated from aqueous solutions (0.005 wt.% for ammonium sulfate and 0.05 wt.% for nigrosin) made with HPLC grade water. A syringe pump (Harvard Apparatus Model 70-2208) injected the solution into an atomizer (TSI Model 3076) with pre-purified N$_2$ as the carrier gas. The aqueous particles were then flowed through several driers to ensure dry particles entered the CRD-AES cell. The relative humidity was monitored in the CRD-AES cell and did not exceed 10%. The spherical nature of both ammonium sulfate and nigrosin dye, generated via drying atomized aqueous solutions, has been confirmed in previous studies
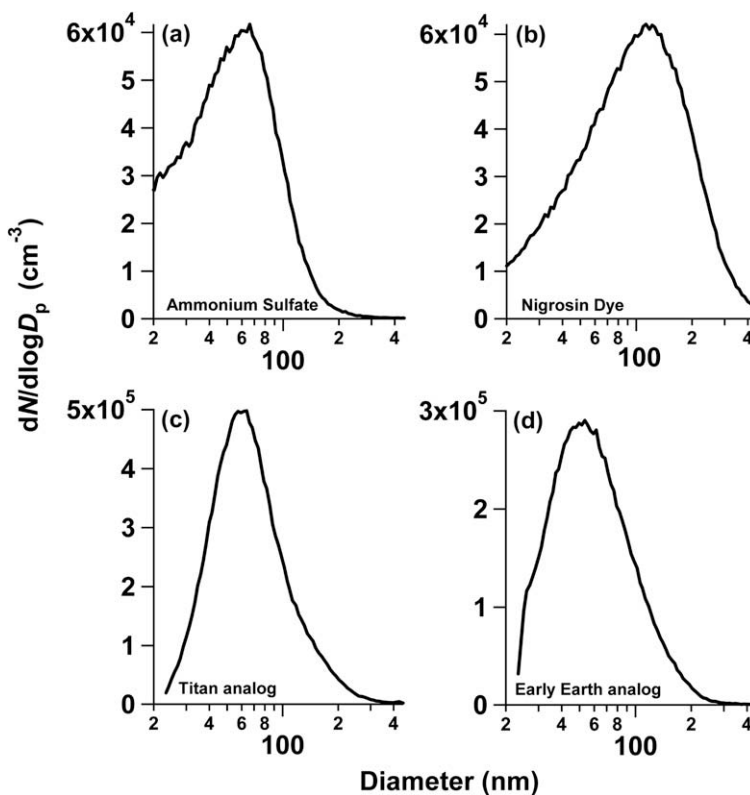

Fig. 3. Representative size distributions of: (a) ammonium sulfate, (b) nigrosin dye, (c) the Titan analog, and (d) the early Earth analog.

(Lack et al., 2006; Wise et al., 2005). The size range for which extinction measurements were made was dictated by the aerosol size distribution. Particles that were smaller than or comparable in diameter to the mode of the size distribution have too much optical interference in the CRD-AES cell from multiply-charged particles. On the other hand, particles much larger than the mode of the size distribution are produced in too few numbers to generate measurable extinction. The size distributions of the test case aerosols are shown in Fig. 3a and b. The mode diameters of the ammonium sulfate and nigrosin dye distributions were 66 nm and 113 nm, respectively.

Extinction coefficients and concentrations for ammonium sulfate particles with diameters from 125 nm to 200 nm, in increments of 25 nm, were measured and corrected for doubly-charged particles. A contour plot of CFD_R values in n–k space for one measurement of ammonium sulfate is shown in Fig. 4a. Fig. 5a shows the extinction efficiency Q_{ext} for the range of ammonium sulfate particle diameters, corrected for doubly-charged particles. The best-fitting refractive index is $n = 1.53 \pm 0.02$ and $k = 0.004 \pm 0.002$, which produced an average CFD_R value of 0.01. This refractive index is almost identical to the accepted refractive index for pure ammonium sulfate of $n = 1.53$ and $k = 0.000$ (Pettersson et al., 2004). Also, the result is similar to other CRD-AES retrieved values in the literature. Riziq et al. (2007) report $n = 1.518$ and $k = 0.002$ using measurements from a pulsed laser CRD-AES. Lang-Yona et al. (2009) report $n = 1.52 \pm 0.01$ and $k = 0.01 \pm 0.01$ for pulsed laser CRD-AES and $n = 1.52 \pm 0.01$ and $k = 0.00 \pm 0.03$ for continuous wave CRD-AES measurements.

For nigrosin dye aerosol, extinction coefficients and concentration of particles with diameters 200–350 nm, in increments of 50 nm, were measured. A contour plot of CFD_R values in n–k space for one measurement of nigrosin dye is shown in Fig. 4b. Fig. 5b shows Q_{ext} versus nigrosin dye particle diameter corrected for doubly-charged particles. The resultant best fit is $n = 1.75 \pm 0.02$ and

$k = 0.338 \pm 0.050$ with an average CFD_R value of 0.02. The retrieved refractive index is comparable to other workers' retrieved values from a variety of techniques. Lack et al. (2006), which used both CRD-AES and photoacoustic spectroscopy, report a retrieved refractive index of nigrosin of $n = 1.70 \pm 0.04$ and $k = 0.31 \pm 0.05$. Riziq et al. (2007) report $n = 1.65 \pm 0.01$ and $k = 0.24 \pm 0.01$. Lang-Yona et al. (2009) report $n = 1.72 \pm 0.01$ and $k = 0.28 \pm 0.08$. The dotted line in Fig. 5b shows the extinction efficiency for the measured refractive index of nigrosin dye aerosol by Lack et al. (2006). The shaded area represents the extreme values of Q_{ext}, calculated from the error in their reported refractive index measurement. The discrepancies that do exist among refractive index measurements of nigrosin dye likely arise from the fact that it is not a pure compound with a defined chemical formula, but rather a mixture of other dyes made as a batch. Our sample has an approximate molecular formula of $C_{49}H_{20}N_7S_3O_{18}$ (elemental analysis performed by Columbia Analytical).

3.2. Refractive index retrieval for Titan and early Earth haze

For both the Titan and early Earth haze analogs, extinction coefficients and concentrations were measured for a size range of 125–200 nm in increments of 25 nm and corrected for doubly-charged particles. The size distributions for the Titan and early Earth aerosols are shown in Fig. 3c and d, respectively. The Titan analog distribution has a mode diameter of 64 nm, and the early Earth analog distribution has a mode diameter of 53 nm. Contour plots of CFD values in n–k space for one measurement of the Titan and early Earth analogs are shown in Fig. 4c and d, respectively. Fig. 6a and b shows Q_{ext} versus diameter corrected for doubly-charged particles. The best fit refractive index for the Titan analog is $n = 1.35 \pm 0.01$ and $k = 0.023 \pm 0.007$, while the early Earth value is $n = 1.81 \pm 0.02$ and $k = 0.055 \pm 0.020$, respectively. The goodness of fit, as assessed by an average CFD_R for three runs consisting of
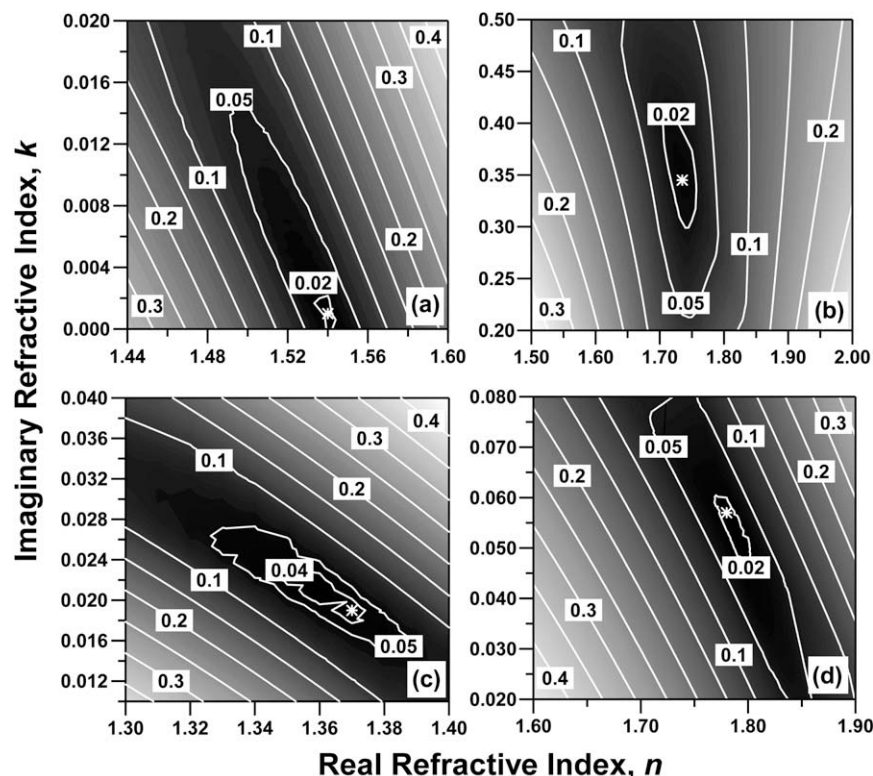

Fig. 4. Example contour plots of CFD_R values in n–k space for one run of each compound: (a) ammonium sulfate, (b) nigrosin dye, (c) Titan analog, and (d) early Earth analog. Unless otherwise indicated, the contours are shown in CFD_R increments of 0.05, and the asterisk represents the lowest CFD_R value of each run.
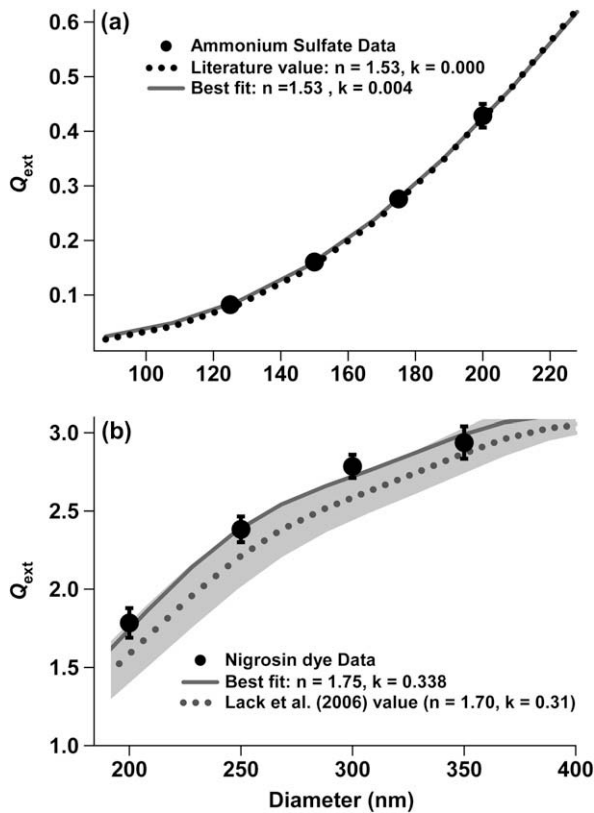
Fig. 5. (a) Extinction efficiency Q_{ext} versus particle diameter for ammonium sulfate. The points show measured data, the solid line shows Q_{ext} calculated for the best fit refractive index of $n = 1.53$ and $k = 0.004$, and the dotted line is for the accepted literature value of $n = 1.53$ and $k = 0.000$. (b) Extinction efficiency Q_{ext} versus particle diameter for nigrosin dye. The points show measured data and the solid line shows Q_{ext} calculated for the best fit refractive index of $n = 1.75$ and $k = 0.338$. The dotted line shows Q_{ext} calculated for the refractive indices retrieved by Lack et al. (2006). The shaded area represents the extreme values of Q_{ext}, calculated from the error reported by Lack et al. (2006) for their refractive index measurements. The extinction efficiencies for both aerosols have been corrected for interference of doubly-charged particles.
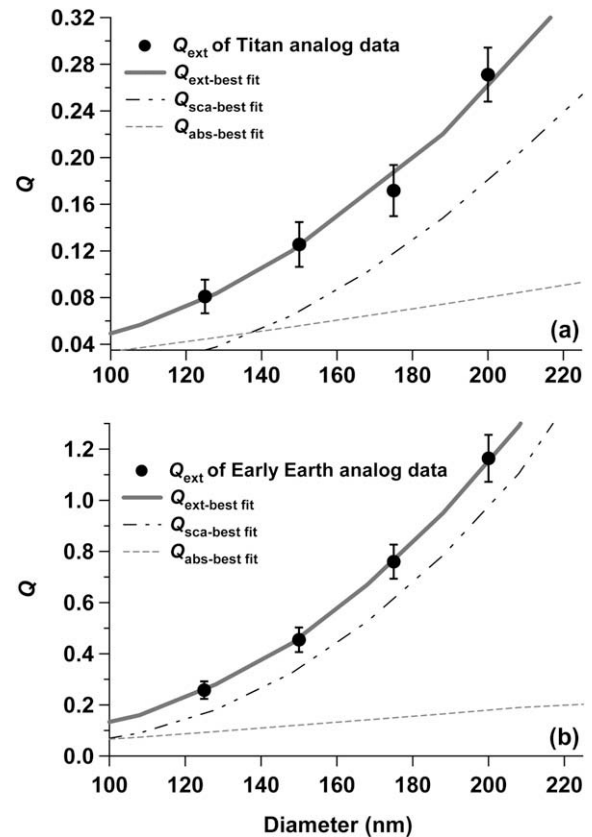

Fig. 6. Extinction efficiency Q_{ext} versus particle diameter for (a) the Titan and (b) early Earth analog aerosols. The points show measured data and the solid line shows Q_{ext} calculated for the best fit refractive index of: (a) $n = 1.35$ and $k = 0.023$ and (b) $n = 1.81$ and $k = 0.055$. The extinction efficiencies have been corrected for interference of doubly-charged particles. Q_{sca} (black dashed line) and Q_{abs} (gray dashed line), calculated from the best fit refractive indices, are also shown.

4. Discussion

4.1. Comparisons of Titan and early Earth optical constants to other studies

Table 1 compares our retrieved refractive indices with previously published Titan aerosol analog refractive indices, linearly interpolated to $\lambda = 532$ nm. All studies differ in their use of energy source, atmospheric mixture, and/or reaction pressure. The Titan analog studied by Khare et al. (1984) was generated by exposing a 10% CH_4 in N_2 gas mixture to an electric discharge at 0.15 Torr. Ramirez et al. (2002) used a cold plasma discharge and a gas mixture of 2% CH_4 in N_2 at 1.5 Torr. The discharge sources used by Khare et al. (1984) and Ramirez et al. (2002) were primarily designed to simulate the chemistry initiated by energetic electrons that impact the top of Titan's atmosphere but do not fully simulate reactions initiated by UV photolysis, also thought to be an important driver in Titan aerosol production (Sagan and Thompson, 1984; Yung et al., 1984). Tran et al. (2003) used a variety of initial gas mixtures containing varying amounts of H_2, CH_4, HC_3N, C_2H_4, C_2H_2, and N_2. The various gas mixtures were exposed to a mercury lamp, which emitted photons at 185 nm and 254 nm. The reaction cell for their experiment was kept at pressures from 100 Torr to 700 Torr. A recent study by Vuitton et al. (2009) used similar experimental conditions to Tran et al. (2003) but used different analysis techniques. Our Titan aerosol analog refractive index has the smallest real refractive index reported, and an imaginary refractive index that is comparable to most of the other values.

four sizes, was 0.04 for the Titan sample, and 0.02 for the early Earth analog.

Fig. 6a and b also shows Q_{sca} and Q_{abs} calculated for the best fit refractive index. For the Titan case, these measured refractive indices indicate that 30–56% of the extinction caused by particles of 125–200 nm diameter is from absorption. In the early Earth case, 15–36% of the extinction is caused by absorption over the same range. In order to verify that enough of the extinction was caused by absorption to determine k, particularly for the early Earth case, we calculated the refractive indices of the two analogs if 100 nm diameter particles were included in the fit. The ratio of absorption to scattering steeply increases as particle diameter decreases, so by including these smaller particles, we could investigate the robustness of our k measurements. Approximately 65% and 51% of the extinction at 100 nm diameter particles is caused by absorption for the Titan and early Earth cases, respectively. Extinction measurements at this diameter were officially excluded since they were considered to be too close to the mode diameters of the analog populations and too influenced by interfering multiply-charged particles. However, when the extinction of the 100 nm particles were included in the fit, the resultant refractive indices for both analogs were within 0.01 of the reported n values and 0.004 of the reported k values. These deviations are well within the error reported.

Table 1

Comparison of measured refractive indices and experimental conditions of this work to other optical constants of Titan analogs studies. All refractive indices from other studies are linearly interpolated to $\lambda = 532$ nm.

Study	n	k	Gas mixture	Energy source	P (Torr)	T (K)
This study, Titan	1.35 ± 0.01	0.023 ± 0.007	0.1% CH_4 in N_2	Continuum UV: $\lambda = 115–400$ nm	630	297
This study, early Earth	1.81 ± 0.02	0.055 ± 0.020	0.1% CH_4 and 0.1% CO_2 in N_2	Continuum UV: $\lambda = 115–400$ nm	630	297
Khare et al. (1984)	1.71 ± 0.04	0.032 ± 0.010	10% CH_4 in N_2	Electrical discharge	0.15	297
Ramirez et al. (2002)	1.569 ± 0.0025	0.0025 ± 0.0009	2% CH_4 in N_2	DC cold plasma discharge	1.5	298
Tran et al. (2003) (Analog A)	1.58	0.054	1.8% CH_4, 0.2% H_2, 0.03% C_2H_4, 0.035% C_2H_2, 0.0017% HC_3N in N_2	Emission line UV: $\lambda = 185$ nm and 254 nm	700	297
Vuitton et al. (2009) (Analog I)	n/a	0.022	Same as in Tran et al. (2003)	Emission line UV: $\lambda = 185$ nm and 254 nm	700	297

Previous chemical analysis indicates that the UV-generated Titan aerosol analog used in the present work contains mostly aliphatic compounds with small amounts of polycyclic aromatic hydrocarbons (PAHs) (Fig. 1). Conversely, electric discharge-generated Titan aerosol formed from a mixture of >1% CH_4 contain significant amounts of PAHs, much larger than aerosol formed from <1% CH_4 (Trainer et al., 2004). The presence of aliphatic compounds in the UV-generated Titan aerosol analog is consistent with recent Visible and Infrared Mapping Spectrometer solar occultation data that show evidence of short aliphatic chains connected to larger hydrocarbons (Bellucci et al., 2009). A typical real refractive index for a straight-chain aliphatic compound is 1.40, while PAHs typically have a higher value of 1.60 (Lide, 1996, p. 3-213, 3-251). Our measured n of 1.35 is closer to that expected for aliphatic species than for aromatics, which is consistent with the chemical fragment pattern observed in Trainer et al. (2006).

There are no direct comparisons to make with the early Earth analog refractive index because such analogs have not been measured previously; however, it has a real refractive index that is higher than all of the Titan analog values, and an imaginary refractive index that is higher than all of the other values except for one case from Tran et al. (2003). The higher real refractive index is expected due to the larger real refractive index found in many oxygenated versus non-oxygenated hydrocarbons in the mid-visible (Lide, 1996, p. 3-26, pp. 3-186–3-187). Interestingly, some HUmic-LIke Substances (HULIS) – oxygenated organics generated from biogenic processes – also have higher k values of 0.023–0.094 (Dinar et al., 2008).

We compare our results more extensively to the groundbreaking work of Khare et al. (1984), since it is most commonly used in both Titan and early Earth atmospheric radiative transfer models and Titan spacecraft-retrieved data analyses (McKay et al., 1989; Pavlov et al., 2001b; Rannou et al., 1997; Tomasko et al., 2008; Toon et al., 1992). Hereafter, we will refer to the Khare et al. (1984) Titan aerosol refractive indices linearly interpolated at $\lambda = 532$ nm as the "Khare values."

Fig. 7 compares the ratio of scattering, absorption, and extinction efficiencies, as well as single-scattering albedos calculated with Mie theory for spherical particles with our retrieved Titan and early Earth refractive indices to the Khare values over a range of particle diameters at $\lambda = 532$ nm. At small sizes ($D < 0.1$ μm), our Titan analog aerosol scatters about 30% of the light that its Khare particle counterpart scatters. The early Earth analog aerosol scatters and extinguishes more light overall than a Khare aerosol of the same size in this range. At a mid-size range (0.1 μm < D < 1 μm), the Titan analog aerosol absorb increasingly less than the Khare aerosol as particle size increases. The Titan aerosol is less scattering and extinguishing than the Khare aerosol until particles reach $D \sim 1$ μm. At this size, the Titan analog aerosol
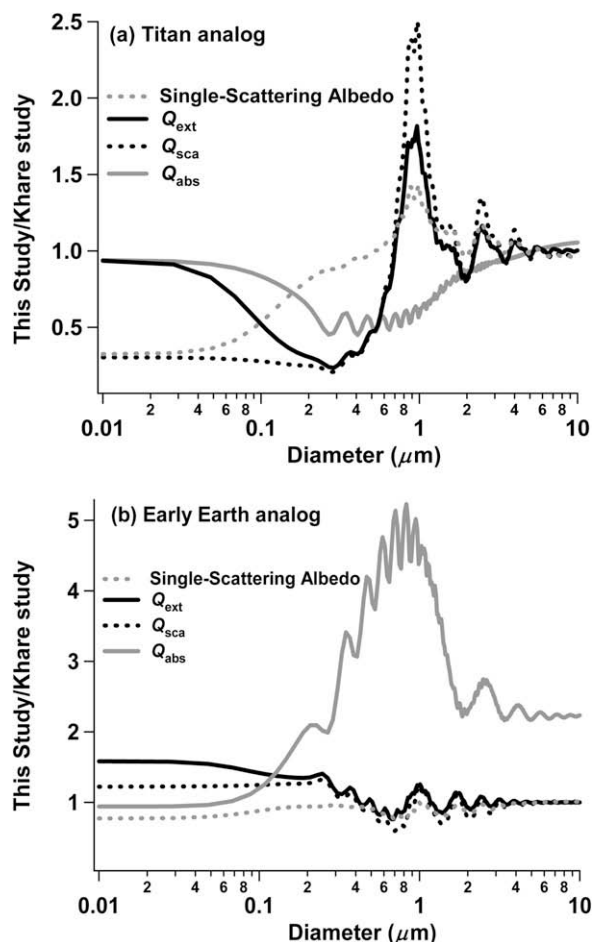

Fig. 7. Ratio of calculated optical properties for spherical particles (single monomers) with refractive indices retrieved from the (a) Titan and (b) early Earth aerosol analogs to those reported by Khare et al. (1984).

scatter and extinguish more light than their Khare counterparts. The absorption of the early Earth aerosol analog is much larger than Khare aerosol of the same size for almost all of the mid-size range. At the largest sizes shown ($D > 1$ μm), there are only small differences between any of the optical efficiencies for the Titan and early Earth analog particles and the Khare ones, except that the absorption efficiency for the early Earth aerosol is about a factor of two larger than the Khare aerosol value. We analyze some of the implications these differences in the refractive index could produce in Titan and early Earth atmospheres in the following section.

4.2. Implications for Titan aerosol

Observations of Titan aerosol indicate that they have a fractal aggregate structure and are typically modeled as particles composed of spherical monomer units attached in irregular patterns (Bellucci et al., 2009; Rannou et al., 1999; Tomasko et al., 2008). We use a semi-empirical fractal aggregate Mie code from Rannou et al. (1999) to compare our retrieved Titan analog refractive indices with the Khare values. The FORTRAN code requires input of monomer size, number of monomer units in an aggregate, incident wavelength of light, fractal dimension, and refractive index. The code outputs the absorption and scattering cross-sections of the aggregates, as well as the asymmetry parameter g. From the absorption and scattering cross-sections, the total extinction cross-section and single-scattering albedo can also be calculated. For our calculations, we assume monomer units with diameters of 100 nm, since this is the size indicated from Huygens probe measurements of linear polarization of the haze (Tomasko et al., 2005) and later confirmed with more detailed analysis by Tomasko et al. (2008) and Bellucci et al. (2009). We assume a fractal dimension of 2 because this is considered to be a typical value for aggregates in Titan's atmosphere, growing under a ballistic cluster–cluster diffusion aggregation process (Rannou et al., 1999).

We compare Q_{ext}, Q_{abs}, Q_{sca}, and g of fractal aggregates, comprised of monomer units that have our retrieved Titan analog refractive indices to ones using the Khare values. Fig. 8 shows the ratio of our calculated optical properties to Khare's for various sized fractal aggregates, where N_m represents the number of monomer units in a fractal aggregate and ranges from 1 to 10,000 units. There is little difference between g obtained for our Titan analog refractive indices and the Khare value for $N_m > 10$. This result is expected, since particles of any composition that are large compared to the incident wavelength of light, spherical or otherwise, are strong forward scatterers (Bohren and Huffman, 1983). There are significant differences in calculated values of the ratios of the optical efficiencies for the entire range of N_m. For a Titan-relevant range of N_m (100–10,000 units; Tomasko et al., 2005, 2008; Bellucci et al., 2009), the ratios of aerosol optical efficiencies using our Titan analog values to Khare's are approximately constant and all less than one. Average values of the ratio of absorption, scattering, and extinction efficiencies using our measured refractive indices compared to ones calculated to the Khare values for $100 \leqslant N_m \leqslant 10{,}000$ are 0.79, 0.25, and 0.30, respectively. In other words, the particles generated in this work are more transparent at the visible wavelength studied than particles having the Khare values. These large differences indicate that inferences made from optical depth retrievals of Titan haze, such as the num-

ber of monomer units, are sensitive to refractive index. For example, it would take triple the number of 100–10,000 monomer unit fractal aggregates composed of Titan aerosol analogs from this work to equal the same extinction at $\lambda = 532$ nm caused by otherwise identical aerosol with refractive indices equaling the Khare values. However, it should be noted that the current state of knowledge of Titan fractal aggregates is only able to constrain the number of monomer units by a factor of 2 at best (Tomasko et al., 2008).

Fig. 9 shows the single-scattering albedo of fractal aggregates ($D = 100$ nm for each monomer unit) calculated using refractive indices from this work, the Khare values, and the Khare values with k increased by a factor of 1.5. This factor has been used to make models of Titan's geometric albedo match observations (Rannou et al., 1995; Toon et al., 1992). The shaded region denotes the range of N_m, from 100 to 10,000 monomer units, that aerosol models require to fit observations (Bellucci et al., 2009; Tomasko et al., 2008). Over the entire range of N_m tested, the single-scattering albedos calculated with the scaled Khare refractive index values fall in between results for the non-scaled Khare values and our Titan aerosol analog values. The fact that the refractive index of these two analog aerosols, generated with different energy sources, yield single-scattering albedos of aggregates above and below what is actually observed on Titan is suggestive. Perhaps the two different types of aerosol formation processes that occur on Titan, one photochemical and the other electrical, result in an observed mixture of two aerosol populations with significantly different optical properties. However, other parameters in addition to energy source, such as analog gas mixture, reaction pressure, and analysis method, also differ between the Khare experimental setup and this work.

4.3. Implications for the early Earth

In order to gauge the effect of the difference between the refractive indices retrieved for the early Earth and Titan analogs, we will use a simple, gray radiative scheme to model the radiation balance of the early Earth atmosphere. This calculation is meant to illustrate how sensitive the early Earth climate may have been to an organic haze in terms of amount of haze material and optical properties. It is not meant to estimate actual conditions on the early Earth.

In a gray radiative scheme, the opacity is considered constant for infrared (IR) and solar radiation. This scheme includes both the greenhouse effect of the constituent gases and the anti-greenhouse effect of the aerosol (Bellucci et al., 2009; McKay et al., 1999). The surface temperature T_S is given by:
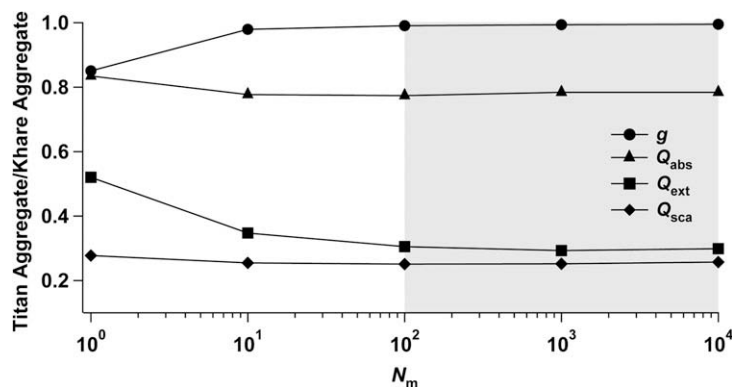

Fig. 8. Ratio of optical properties of fractal aggregate aerosol containing monomer units with refractive indices retrieved from the Titan aerosol analogs in this work to those reported by Khare et al. (1984). The shaded region represents the physically relevant range of monomer units per aggregate fractal that aerosol models have inferred from spacecraft observations.
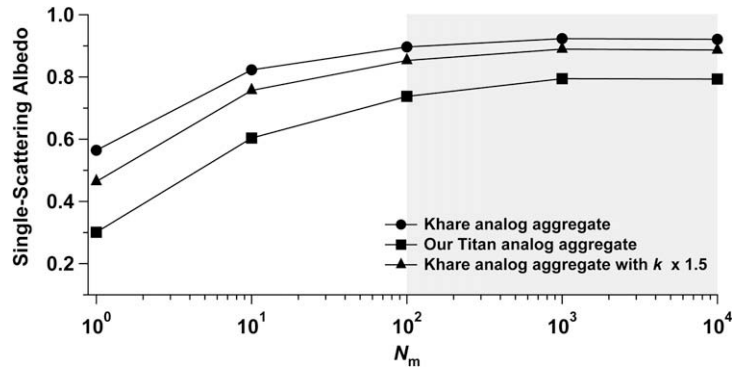
Fig. 9. Single-scattering albedo of fractal aggregate aerosol containing monomer units with refractive indices retrieved from the Titan aerosol analogs in this work and those reported by Khare et al. (1984). The circles denote values calculated for aggregates using Khare values, squares denote values calculated for aggregates using the Titan aerosol analog refractive index reported in this work, and the triangles denote values calculated from the Khare values with the imaginary refractive index multiplied by a factor of 1.5. The shaded region represents the physically relevant range of monomer units per aggregate fractal that aerosol models have inferred from spacecraft observations.

$$\sigma T_S^4 = (F_g + (1 - \gamma)F_s)\left(1 + \frac{3}{4}\tau^*\right) + \frac{\gamma F_s}{2} \tag{4}$$

where σ is the Stefan–Boltzmann constant, F_g is the geothermal heat term, τ^* is the IR opacity, and F_s is the incident sunlight absorbed at the surface and averaged over the disk. F_s can be expressed as $(1 - a)F_0/4$, where F_0 is the solar constant and a is the albedo. The fraction of incident light (not reflected out to space) that is absorbed by the stratospheric haze layer is defined as γ. Mathematically, we can define γ in terms of the total reflectance of a layer R, total absorbance A, and total transmittance T (where $T = 1 - R - A$):

$$\gamma = \frac{A}{1 - R} \tag{5}$$

We can define $R = 2\beta\tau_{sca}$ and $A = 2\tau_{abs}$, where β is the fraction of incident light that is scattered into the upper hemisphere and τ_{sca} and τ_{abs} are the scattering and absorption optical depths, respectively (Chylek and Wong, 1995). An optical depth τ of any kind is equivalent to $C\rho_c$, where C is an optical cross-section (cm^2 particle^{-1}) and ρ_c is the column density (particles cm^{-2}). Substituting these terms into Eq. (5), γ can be written as:

$$\gamma = \frac{C_{abs}}{0.5\rho_c^{-1} - \beta C_{sca}} \tag{6}$$

In the following calculations, β is approximated as $(1 - 0.5g)/2$, where g is the asymmetry parameter, as done by Sagan and Pollack (1967) and Chylek and Wong (1995). Eq. (6) allows us to calculate γ for aerosol with different refractive indices, since both scattering (C_{sca}) and absorption (C_{abs}) optical cross-sections of spherical particles are functions of refractive index. By combining Eqs. (4) and (6), the surface temperature of the early Earth can be calculated as a function of IR opacity and particle column density.

Fig. 10 shows a contour plot of surface temperature (in degrees K) for varied values of IR opacity and particle column density for the early Earth using three different aerosol refractive indices: the Khare values and our Titan and early Earth organic haze aerosol analog values. The corresponding values of γ are shown on the top axis of each plot. For a given IR opacity, increasing column density decreases the surface temperature. In all three scenarios, as γ approaches its maximum value of 1, corresponding to a complete anti-greenhouse, the surface temperature asymptotically reaches its physically allowable minimum surface temperature of $\frac{1}{\sqrt{2}}$ of the effective temperature (McKay et al., 1999). In the case of an early Earth experiencing 80% of present day solar irradiance, this minimum temperature is approximately 202 K. The difference among these three scenarios is the amount of particles needed to
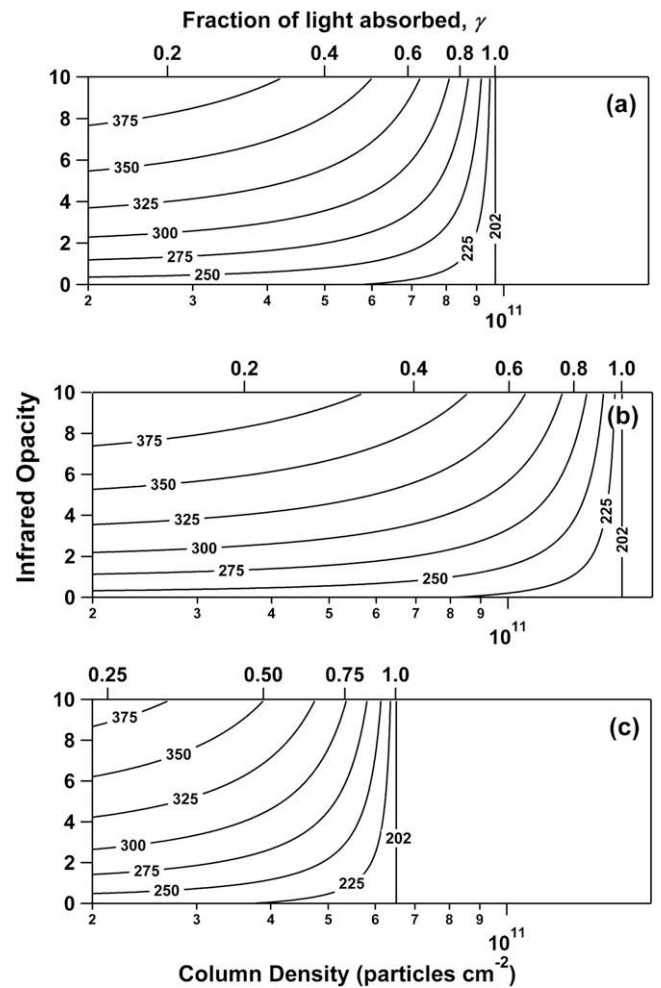

Fig. 10. Contour plots of early Earth surface temperature (in degrees K) for a range of IR opacities and aerosol particle column densities. The particles are assumed to be 100 nm diameter spheres. The top axis shows values of γ that correspond to column densities. Each plot assumes different values of the refractive indices of the particles: (a) Khare et al. (1984) values, (b) Titan analog values from this work, and (c) early Earth analog values from this work.

induce this anti-greenhouse effect observed for a given IR opacity. The early Earth case requires approximately 30% fewer particles to reach γ of 1 than the Khare analog case and 60% fewer than the Titan analog case. For column densities greater than 2×10^{10}

particles cm^{-2}, there are significant differences among the three scenarios. For instance, if the early Earth had an IR opacity of 1, the surface temperature with no haze layer present would be 276 K. If it also had an organic haze of 2.5×10^{10} haze particles cm^{-2}, the surface temperature in the three cases would be approximately 261 K, 267 K, and 269 K assuming refractive indices of the early Earth analog aerosol, the Titan analog aerosol, and Khare analog aerosol, respectively. These temperature depressions are comparable to the 10 K anti-greenhouse effect on Titan and to cooling predicted for nuclear winter scenarios involving soot injected into the stratosphere on present day Earth (Robock et al., 2007). However, much smaller and larger differences are possible, all dependent upon the amount of haze material present.

These calculations are not meant to show hypothesized early Earth surface temperatures for the three cases; realistic values require detailed aerosol models to determine appropriate particle size, concentration, structure (spherical versus aggregate), and distribution throughout the atmosphere. Rather, the purpose of this calculation is to illustrate the large differences in radiative impacts that the refractive index of each aerosol type have, emphasizing the importance of incorporating the most appropriate optical properties for a given type of aerosol into early Earth radiative transfer models. For future studies, we are planning on expanding this single measurement of n and k in the mid-visible to the UV and IR. Measurements of n and k at this single wavelength will enable us to conduct future optical hygroscopic growth studies of early Earth aerosol. These studies will help to more fully understand the effect these aerosol may have had on the radiative balance of the early Earth atmosphere.

5. Conclusion

We have measured refractive indices at λ = 532 nm for two organic aerosol analogs. One is relevant for aerosol generated by UV photolysis in the atmosphere of Titan, while the other is relevant for aerosol that may have been photolytically produced in a mildly reducing early Earth atmosphere. For our Titan analog particles, we find a real refractive index of n = 1.35 ± 0.01 and an imaginary refractive index k = 0.023 ± 0.007, and for the early Earth analog particles we find n = 1.81 ± 0.02 and k = 0.055 ± 0.020. The results indicate that Titan analog aerosol from this study have a lower real refractive index and a similar imaginary refractive index compared to values reported in Khare et al. (1984). For a given amount of extinction, three times as many fractal aggregates composed of 100–10,000 monomer 100 nm diameter units having the Titan analog refractive index from this study would be needed compared to identically-sized particles having the Khare value. The measurements of the early Earth aerosol analog indicate that the incorporation of oxygen into the particles greatly increases the refractive index of the particle. According to our simple radiative scheme of the early Earth atmosphere, these early Earth organic aerosol have a profoundly harsher anti-greenhouse effect than their Titan counterparts.

References

Bellucci, A., Sicardy, B., Drossart, P., Rannou, P., Nicholson, P.D., Hedman, M., Baines, K.H., Burrati, B., 2009. Titan solar occultation observed by Cassini/VIMS: Gas absorption and constraints on aerosol composition. Icarus 201, 198–216.
Bohren, C.F., Huffman, D.R., 1983. Absorption and Scattering of Light by Small Particles. John Wiley & Sons, Inc. p. 115.
Burgdorf, M., Orton, G., van Cleve, J., Meadows, V., Houck, J., 2006. Detection of new hydrocarbons in Uranus' atmosphere by infrared spectroscopy. Icarus 184, 634–637.
Cabane, M., Chassefiere, E., 1995. Laboratory simulations of Titan's atmosphere – Organic gases and aerosols. Planet. Space Sci. 43, 47–65.
Chylek, P., Wong, J., 1995. Effect of absorbing aerosols on global radiation budget. Geophys. Res. Lett. 22, 929–931.
DeWitt, H.L., Trainer, M.G., Pavlov, A.A., Hasenkopf, C.A., Aiken, A.C., Jimenez, J.L., McKay, C.P., Toon, O.B., Tolbert, M.A., 2009. Reduction in haze formation rate on prebiotic Earth in the presence of hydrogen. Astrobiology 9, 447–453.
Dinar, E., Riziq, A.A., Spindler, C., Erlick, C., Kiss, G., Rudich, Y., 2008. The complex refractive index of atmospheric and model humic-like substances (HULIS) retrieved by a cavity ring down aerosol spectrometer (CRD-AS). Faraday Discuss. 137, 279–295.
Domagal-Goldman, S.D., Kasting, J.F., Johnston, D.T., Farquhar, J., 2008. Organic haze, glaciations and multiple sulfur isotopes in the Mid-Archean Era. Earth Planet. Sci. Lett. 269, 29–40.
Gillett, F.C., Forrest, W.J., 1974. 7.5- to 13.5-micron spectrum of Saturn. Astrophys. J. 187, L37–L39.
Grainger, R.G., Lucas, J., Thomas, G.E., Ewen, G.B.L., 2004. Calculation of Mie derivatives. Appl. Opt. 43, 5386–5393.
Haqq-Misra, J.D., Domagal-Goldman, S.D., Kasting, P.J., Kasting, J.F., 2008. A revised, hazy methane greenhouse for the Archean Earth. Astrobiology 8, 1127–1137.
Hord, C.W., West, R.A., Simmons, K.E., Coffeen, D.L., Sato, M., Lane, A.L., Bergstralh, J.T., 1979. Photometric-observations of Jupiter at 2400-angstroms. Science 206, 956–959.
Kasting, J.F., Zahnle, K.J., Walker, J.C.G., 1983. Photochemistry of methane in the Earth's early atmosphere. Precambrian Res. 20, 121–148.
Khare, B.N., Sagan, C., Arakawa, E.T., Suits, F., Callcott, T.A., Williams, M.W., 1984. Optical-constants of organic tholins produced in a simulated titanian atmosphere – From soft-X-ray to microwave-frequencies. Icarus 60, 127–137.
Kim, S.J., Caldwell, J., Rivolo, A.R., Wagener, R., Orton, G.S., 1985. Infrared polar brightening on Jupiter: III. Spectrometry from the Voyager-1 IRIS experiment. Icarus 64, 233–248.
Lack, D.A., Lovejoy, E.R., Baynard, T., Pettersson, A., Ravishankara, A.R., 2006. Aerosol absorption measurement using photoacoustic spectroscopy: Sensitivity, calibration, and uncertainty developments. Aerosol Sci. Technol. 40, 697–708.
Lang-Yona, M., Rudich, Y., Segre, E., Dinar, E., Abo-Riziq, A., 2009. Complex refractive indices of aerosols retrieved by continuous wave-cavity ring down aerosol spectrometer. Anal. Chem. 81, 1762–1769.
Lide, D. (Ed.), 1996. CRC, Handbook of Chemistry and Physics. John Wiley and Sons, Cleveland.
McKay, C.P., Pollack, J.B., Courtin, R., 1989. The thermal structure of Titan's atmosphere. Icarus 80, 23–53.
McKay, C.P., Pollack, J.B., Courtin, R., 1991. The greenhouse and antigreenhouse effects on Titan. Science 253, 1118–1121.
McKay, C.P., Lorenz, R.D., Lunine, J.I., 1999. Analytic solutions for the antigreenhouse effect: Titan and the early Earth. Icarus 137, 56–61.
Moses, J.I., Rages, K., Pollack, J.B., 1995. An analysis of Neptune stratospheric haze using high-phase-angle Voyager images. Icarus 113, 232–266.
Pavlov, A.A., Kasting, J.F., Brown, L.L., Rages, K.A., Freedman, R., 2000. Greenhouse warming by CH_4 in the atmosphere of early Earth. J. Geophys. Res. Planets 105, 11981–11990.
Pavlov, A.A., Brown, L.L., Kasting, J.F., 2001a. UV shielding of NH_3 and O_2 by organic hazes in the Archean atmosphere. J. Geophys. Res. Planets 106, 23267–23287.
Pavlov, A.A., Kasting, J.F., Eigenbrode, J.L., Freeman, K.H., 2001b. Organic haze in Earth's early atmosphere: Source of low-C-13 Late Archean kerogens? Geology 29, 1003–1006.
Pettersson, A., Lovejoy, E.R., Brock, C.A., Brown, S.S., Ravishankara, A.R., 2004. Measurement of aerosol optical extinction at 532 nm with pulsed cavity ring down spectroscopy. J. Aerosol Sci. 35, 995–1011.
Ramirez, S.I., Coll, P., da Silva, A., Navarro-Gonzalez, R., Lafait, J., Raulin, F., 2002. Complex refractive index of Titan's aerosol analogues in the 200–900 nm domain. Icarus 156, 515–529.
Rannou, P., Cabane, M., Chassefiere, E., Botet, R., McKay, C.P., Courtin, R., 1995. Titan's geometric albedo: Role of the fractal structure of the aerosols. Icarus 118, 355–372.
Rannou, P., Cabane, M., Botet, R., Chassefiere, E., 1997. A new interpretation of scattered light measurements at Titan's limb. J. Geophys. Res. Planets 102, 10997–11013.
Rannou, P., McKay, C.P., Botet, R., Cabane, M., 1999. Semi-empirical model of absorption and scattering by isotropic fractal aggregates of spheres. Planet. Space Sci. 47, 385–396.

Riziq, A.A., Erlick, C., Dinar, E., Rudich, Y., 2007. Optical properties of absorbing and non-absorbing aerosols retrieved by cavity ring down (CRD) spectroscopy. Atmos. Chem. Phys. 7, 1523–1536.

Robock, A., Oman, L., Stenchikov, G.L., Toon, O.B., Bardeen, C., Turco, R.P., 2007. Climatic consequences of regional nuclear conflicts. Atmos. Chem. Phys. 7, 2003–2012.

Sagan, C., Chyba, C., 1997. The early faint Sun paradox: Organic shielding of ultraviolet-labile greenhouse gases. Science 276, 1217–1221.

Sagan, C., Pollack, J.B., 1967. Anisotropic nonconservative scattering and clouds of Venus. J. Geophys. Res. 72, 469–477.

Sagan, C., Thompson, W.R., 1984. Production and condensation of organic gases in the atmosphere of Titan. Icarus 59, 133–161.

Smith, B.A., and 26 colleagues, 1981. Encounter with Saturn – Voyager-1 imaging science results. Science 212, 163–191.

Tomasko, M.G., and 39 colleagues, 2005. Rain, winds and haze during the Huygens probe's descent to Titan's surface. Nature 438, 765–778.

Tomasko, M.G., Doose, L., Engel, S., Dafoe, L.E., West, R., Lemmon, M., Karkoschka, E., See, C., 2008. A model of Titan's aerosols based on measurements made inside the atmosphere. Planet. Space Sci. 56, 669–707.

Toon, O.B., McKay, C.P., Griffith, C.A., Turco, R.P., 1992. A physical model of Titan's aerosols. Icarus 95, 24–53.

Trainer, M.G., Pavlov, A.A., Jimenez, J.L., McKay, C.P., Worsnop, D.R., Toon, O.B., Tolbert, M.A., 2004. Chemical composition of Titan's haze: Are PAHs present? Geophys. Res. Lett. 31, 404–419.

Trainer, M.G., Pavlov, A.A., DeWitt, H.L., Jimenez, J.L., McKay, C.P., Toon, O.B., Tolbert, M.A., 2006. Organic haze on Titan and the early Earth. Proc. Natl. Acad. Sci. 103, 18035–18042.

Tran, B.N., Joseph, J.C., Ferris, J.P., Persans, P.D., Chera, J.J., 2003. Simulation of Titan haze formation using a photochemical flow reactor – The optical constants of the polymer. Icarus 165, 379–390.

Vuitton, V., Tran, B.N., Persans, P.D., Ferris, J.P., 2009. Determination of the complex refractive indices of Titan haze analogs using photothermal deflection spectroscopy. Icarus 203, 663–671.

Wiedensohler, A., 1988. An approximation of the bipolar charge-distribution for particles in the sub-micron size range. J. Aerosol Sci. 19, 387–389.

Wise, M.E., Biskos, G., Martin, S.T., Russell, L.M., Buseck, P.R., 2005. Phase transitions of single salt particles studied using a transmission electron microscope with an environmental cell. Aerosol Sci. Technol. 39, 849–856.

Yung, Y.L., Allen, M., Pinto, J.P., 1984. Photochemistry of the atmosphere of Titan – Comparison between model and observations. Astrophys. J. Suppl. Ser. 55, 465–506.

Zahnle, K.J., 1986. Photochemistry of methane and the formation of hydrocyanic acid (HCN) in the Earth's early atmosphere. J. Geophys. Res. Atmos. 91, 2819–2834.